

Quantifying the thermal dynamics of a permafrost site near Ny-Ålesund, Svalbard

Kurt Roth

Institute of Environmental Physics, University of Heidelberg, Heidelberg, Germany

Julia Boike¹

Alfred-Wegener-Institute for Polar and Marine Research, Potsdam, Germany

Abstract. The dynamics of permafrost soils is manifest in the soil temperature which can be measured with high accuracy and high temporal resolution. Using continuous data over a period of 778 days from a mineral hummock field at the Bayelva site, Svalbard, we deduce and quantify the processes which constitute the dynamics. In particular, conductive heat flux, generation of heat from phase transitions, and migration of water vapor are analyzed. Support for the interpretation of the data comes from high-resolution time domain reflectometry measurements of the liquid water content.

1. Introduction

Permafrost underlies about one fifth of global land areas [French, 1996] and hence constitutes an important terrestrial system. Models indicate that high-latitude regions are affected most strongly by a change of the climate, and warming has actually been reported in several studies [Overpeck *et al.*, 1997; Huang *et al.*, 2000; Serreze *et al.*, 2000]. Quantitative understanding of the processes underlying the thermal and hydraulic dynamics of permafrost soils is thus paramount to anticipate consequences of a changing atmospheric forcing as well as to improve the parameterization of the soil-atmosphere interaction in climate models.

The major stages for the seasonal thermal dynamics of the active layer at a permafrost site are a winter cold period when the soil is completely frozen, a warming period when snow melts and possibly infiltrates into the still frozen soil, a downward moving thaw front during the summer thaw period, and an isothermal plateau during the fall freeze back.

Conduction is widely accepted to be the dominant mechanism of heat transfer in soils. Other nonconductive heat transfer mechanisms associated with the convection of water, either in the liquid or in the vapor phase, are possible with appropriate gradients. The significance of conductive and convective heat transfer for the thermal dynamic of permafrost and active layer has been discussed in numerous, and often controversial, publications. Conduction is assumed to be the dominant heat transfer process during the winter cold period, although the possibility of convection in frozen soil has been reported in field and lab experiments [Parmuzina, 1978; Chen and Chamberlain, 1988]. When the snow cover becomes isothermal and snowmelt starts during the warming period, the soil rapidly warms at all depths, presumably because of the infiltration and refreezing of snowmelt water and of migrating vapor into the frozen soil. Most studies agree that nonconductive heat trans-

fer processes must be responsible for the rapid warming of the soil [Putkonen, 1998; Hinkel and Outcalt, 1994]. Conversion of latent heat is thought to be most important during the summer when moisture evaporates from the surface and the active layer thaws. Evaporation consumes 25–50% of the total incoming energy at a Siberian study site [Boike *et al.*, 1998] and 30–65% in northern Alaska [Kane *et al.*, 1990]. According to Outcalt *et al.* [1998], evaporative cooling at the surface of the active layer was responsible for the deviation between observed and modeled soil temperatures of the active layer and upper permafrost. Thawing of the active layer is another important sink for thermal energy. It consumes up to 40% of the total net radiation at the Siberian site of Boike *et al.* [1998]. Generally, a high percentage of the total heat flux into the ground (between 70 and 100%) is converted into latent heat [Rouse, 1984; Boike *et al.*, 1998].

Besides conduction of heat, transport of thermal energy by convection of water, either in the liquid or vapor phase, has been discussed. Hinkel *et al.* [1993] identified infiltration of summer precipitation as an effective method to transfer heat to the base of the active layer, especially in drained, organic soils. Pore water convection during the summer thaw period, driven by the density inversion of water, has been proposed as the initiator for the formation of sorted circles [Krantz, 1990; Ray *et al.*, 1983], but Hallet [1990] argued that this process is unlikely and that it has not been observed in finer-grained sediments typically found in patterned ground. Putkonen [1998] calculated a Peclet number much smaller than 1 for this site and concluded that advection of heat due to water motion is negligible.

When net radiation decreases during the fall, the soil is cooled to a practically isothermal condition, the so-called zero curtain at 0°C. The large amount of latent heat which must be removed from the profile through an almost isothermal soil stabilizes soil temperatures at 0°C for a prolonged time. Hinkel and Outcalt [1993, 1994] suggested that internal distillation driven by osmotic gradients transfer heat across this isothermal zone. In contrast, Romanovsky and Osterkamp [2000] accurately predicted soil temperatures during the freeze back using a conductive heat exchange model by including effects of unfrozen water and therefore excluding moisture migrating as a

¹On leave at Water and Environmental Research Center, University of Alaska, Fairbanks, Alaska, USA.

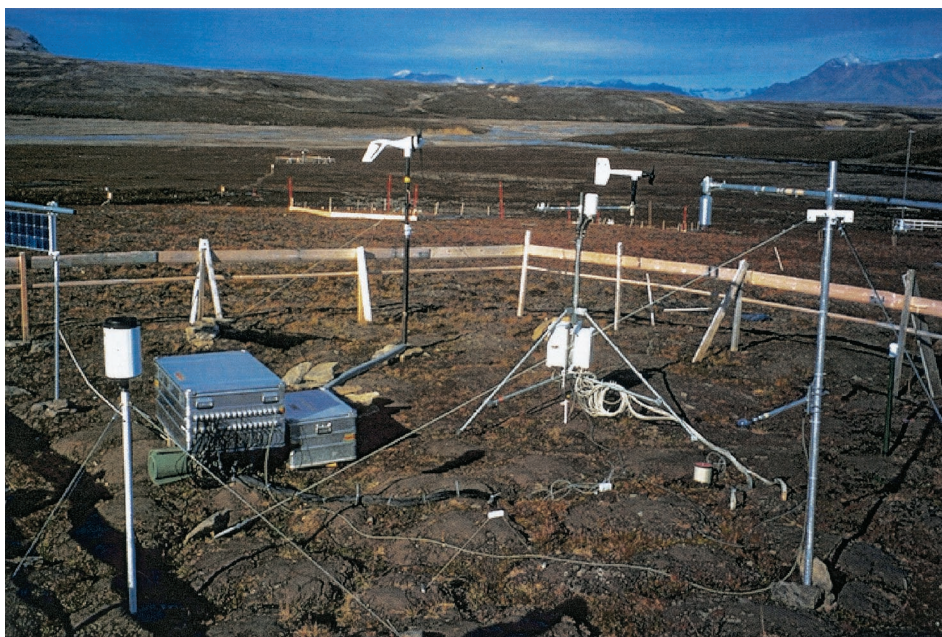


Plate 1. View of the experimental site with Bayelva river in the background. Instruments visible are, from left to right, solar power panel, rain gauge, boxes with electronics and batteries, wind generator, weather station, snow height sensor, and net radiation sensor.

transport mechanism. *Putkonen* [1998] estimated that the maximal possible vapor and latent heat flux under given soil thermal properties was >2 orders of magnitude smaller than conductive heat transport, hence being insignificant. The eventual progress of the frost front is governed by the spatial heterogeneity of the soil [*Boike et al.*, 1998].

Experimental identification and quantification of heat transfer processes in permafrost soils is hampered by the lack of accurate methods for measuring relevant state variables of the system, for example the phase density of ice or water vapor, and even more so by the lack of sufficiently accurate instruments for measuring fluxes of thermal energy and of water. We are thus left with deducing process hypotheses based on the internal consistency of incomplete data sets. This situation is not alleviated significantly by numerical simulations which still suffer from incomplete representation of physical processes, such as the separation of the water phase upon freezing of the porous medium, and by typically inaccurate parameterizations of material properties, such as the conductivity for liquid water and vapor. As a consequence, detailed case studies are required to gain the type of knowledge prerequisite for assessing the impact of a changing atmospheric forcing on permafrost soils as well as the ensuing feedback on the atmosphere.

Apart from the relevance outlined so far, the dynamics of permafrost soils is of inherent scientific interest because it encompasses highly nonlinear and strongly coupled processes which lead to a complex phenomenology. Understanding such a system quantitatively will not only improve conceptualizations of terrestrial permafrost and its role in a dynamic environment, it is also pertinent to discussions about the environments of other planets, for example, to recent questions about water on Mars [*Costard*, 1988; *Zuber et al.*, 1998].

In this paper we demonstrate an approach for exploring the thermal dynamics of a continuous permafrost site using a time series of soil temperature. Our goals are (1) to examine the soil thermal processes using bulk thermal properties and (2) to

quantitatively examine soil heat transfer processes through the annual cycles using high-resolution soil temperature and moisture data.

2. Site Description and Measured Data

The Bayelva catchment is located ~ 3 km west of Ny-Ålesund, Svalbard, at ($78^{\circ}55'N$, $11^{\circ}50'E$). Continuous permafrost in this region underlies coastal areas to depths of ~ 100 m and mountainous areas to depths >500 m [*Liestøl*, 1977]. The North Atlantic Current warms this area to an average air temperature $\sim 5^{\circ}C$ in July and $-13^{\circ}C$ in January, and it provides ~ 400 mm of annual precipitation that mostly falls as snow between September and May [*Førland et al.*, 1997].

Our study site is located some 30 m above mean sea level, on top of a small hill covered with unsorted circles (Plate 1). The bare inner part of the soil circle is ~ 1 m in diameter and is surrounded by vegetated borders consisting of a mixture of low vascular plants, mosses, and lichens. We instrumented one of these circles in August 1998 to automatically monitor hourly temperature and half-daily liquid water content. Soil temperatures are recorded using thermistors calibrated at $0^{\circ}C$ with a precision of $0.00024^{\circ}C$ at $0^{\circ}C$ and an absolute error less than $\pm 0.02^{\circ}C$ over the temperature range $\pm 30^{\circ}C$. Liquid water content is calculated from time domain reflectometry (TDR) measurements using the semiempirical mixing model of *Roth et al.* [1990] which was augmented by including ice as the fourth phase. The accuracy of the measurement of volumetric water content by TDR is estimated to be between 0.02 and 0.05, while its precision is better than 0.005. A weather station measuring solar radiation, net radiation, air temperature, snow depth, and rainfall stands within 5 m of the instrumented soil site. Field accuracy of the net radiation measurements is estimated to range between 10 and 20% of the measured value.

During installation, soil samples were taken for the analysis of physical properties. The soil consists of silty clay with inter-

spersed stones. Clay content by weight increases from 20% near the surface to 80% at 0.8 m depth with a corresponding decrease of silt and sand content. The average soil bulk density obtained from six samples is $1.70 \times 10^3 \text{ kg m}^{-3}$ with porosity ranging from 0.36 to 0.5.

In this paper we are using data from temperature sensors and TDR probes installed in the circle's center at depths 0.065, 0.245, 0.405, 0.625, 0.765, 0.995, 1.125, and 1.250 m below the surface (Plate 2). Hourly data collection started in September 1998. The data spans over 2 years, from September 14, 1998 (day 257), to October 31, 2000 (day 1035), which results in measured values for $\sim 18,500$ points in time. In order to reduce the amount of data we used the linear hat filter

$$\bar{f}(t_k) := \sum_{i=-n}^n w(i) f(t_{k+i}) \bigg/ \sum_{i=-n}^n w(i) \quad w(i) := 1 - |i/n|, \quad (1)$$

where f is the quantity to be averaged, w is the weight function, and \bar{f} is the averaged value. For our data we chose $n = 12$, which results in a temporal resolution of 12 hours. We remark that the final results are not affected by the order of filtering and analysis, which will be described in section 4, since both are linear. We thus applied the filter prior to the analysis.

Through both winters, the snow cover built up in two stages, first to a height of ~ 0.3 m then to ~ 0.7 m. They differ significantly in the duration of these two stages, however. During the first winter, the thin snow cover lasted some 50 days, and the thick one lasted for some 130 days. During the second winter, the lengths of the periods were reversed: almost 190 days for the thin and only 70 days for the thick cover. Since average air temperature and net radiation during both winters were comparable, the thinner snow cover caused a considerably stronger cooling of the soil. The minimum soil temperatures at 0.5 m depth were below -15°C .

During the first year, days 264–619, the average net radiative input was $+13.4 \text{ W m}^{-2}$, while during the second year, days 620–986, it was -2.4 W m^{-2} . Mean air temperatures were comparable for these periods: -4.4°C and -5.6°C , respectively. Together with the longer duration of the snow-free ground in the first summer this atmospheric forcing led to a deeper and prolonged thawing of the active layer.

Soil temperatures exhibit the characteristic behavior of the freeze-thaw cycle that has already been described for other sites, for example, by *Boike et al.* [1998]. The active layer thaws gradually during the summer, at this study site to depths between 0.9 and 1.1 m. Freeze back occurs in succinctly different steps. First, temperatures drop to 0°C throughout the thawed zone, around days 628 and 990, respectively, at this site, which is often referred to as the zero curtain [*Outcalt et al.*, 1990]. This phenomenon practically eliminates conductive heat transfer because of the vanishing thermal gradient. In the second step a wide, almost isothermal plateau with temperatures between 0 and -2°C develops, which becomes slowly eroded from above as well as from below. The isothermal regime ends at a cold front that encroaches from the surface at a speed that is comparable to that of the thawing front in summer. This front is most prominent at the onset of the second winter between days 690 and 720. Afterward, temperatures drop rapidly.

As expected, liquid water content is highest near the bottom of the thawed zone where the frozen soil and the ice form an impermeable layer. Water contents during the second summer are much higher than during the first one because of signifi-

cantly higher precipitation. Looking at the transition from the thawed to the frozen state, we notice that passing the 0°C line does not appear to noticeably affect the liquid water content. Instead, it decreases very slowly across the isothermal sub-freezing plateau and only drops to small values with the passing of the winter's cold front. Liquid water exists in this profile even with temperatures below -15°C . This has also been reported for other sites [e.g., *Farouki*, 1981; *Romanovsky and Osterkamp*, 2000].

3. Theory

Conservation of thermal energy in a one-dimensional system may be formulated as

$$\frac{\partial}{\partial t} [c_h T] + \frac{\partial}{\partial z} j_h = r_h, \quad (2)$$

where c_h is heat capacity, T is temperature, z is depth, j_h is heat flux, and r_h is the rate of heat production. For purely conductive transport of heat, to which we will restrict our analysis, the flux is described by Fourier's law

$$j_h = -k_h \frac{\partial}{\partial z} T, \quad (3)$$

where k_h is the bulk thermal conductivity. For the most simple case of a stationary homogeneous soil these equations may be combined to obtain the diffusion equation

$$\frac{\partial}{\partial t} T - d_h \frac{\partial^2}{\partial z^2} T = \frac{r_h}{c_h}, \quad (4)$$

where

$$d_h = \frac{k_h}{c_h} \quad (5)$$

is the thermal diffusivity. Analytical solutions of (4) are available for a wide range of flow geometries and boundary conditions [*Carslaw and Jaeger*, 1990; *Crank*, 1975].

The diffusion equation (4) is based on the tacit assumption that the medium considered is a single-phase system, such as a solid, which is described in the continuum limit. The values of the material properties c_h and d_h may then be calculated from first principles. For the case of a multiphase system like a permafrost soil, (4) is only retrieved after averaging over a sufficiently large region [e.g., *Hassanizadeh and Gray*, 1979], and the material properties become dependent on the volume fractions of the constituting phases as well as on their geometry. The heat capacity is obtained easily by summing the contributions of the phases, i.e.,

$$c_h = \sum_k \theta_k \rho_k c_{hk}, \quad (6)$$

where θ_k , ρ_k , and c_{hk} are volume fraction, mass density, and heat capacity per unit mass, respectively, of phase k . In contrast, the thermal diffusivity d_h depends on the geometry of the phases in a complicated way. It is often parameterized using the model of *Philip and de Vries* [1957].

In this work we assume the structure of the soil to be such that averaging the pore-scale processes will, indeed, produce a diffusion equation for the dynamics of heat transport, and we will consider the material properties c_h and d_h as bulk properties.

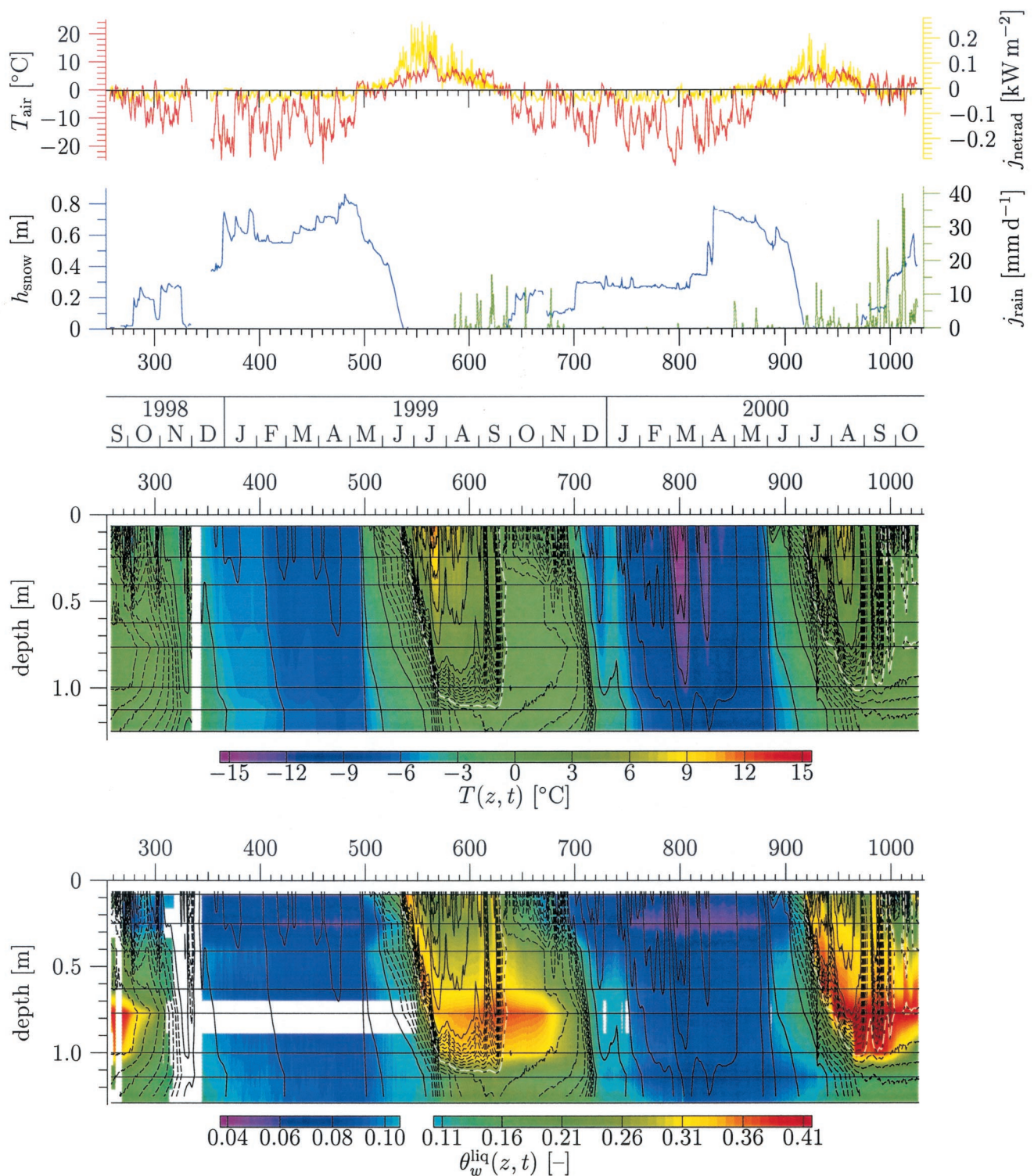


Plate 2. (top) Measured meteorological variables, (middle) soil temperature $T(z, t)$, and (bottom) volumetric water content $\theta_w^{\text{iiq}}(z, t)$ after averaging over ± 12 hours with the linear hat filter (1). Rainfall data are only available after day 578. Contour lines of soil temperature are drawn with increments of 2°C (solid line) and 0.2°C (dashed line), respectively, around 0°C (black-and-white-dashed lines). These lines are repeated in the plots of θ_w^{iiq} and all subsequent contour plots to facilitate cross-referencing. Time is given in Julian days starting January 1, 1998, as well as by month and year. Open areas indicate missing data, and horizontal black lines indicate the positions of the probes.

For the case of negligible heat production, $r_h = 0$, the solution of (4) in a semi-infinite medium with initial temperature $T = 0$ and surface temperature $T(0, t)$ is given by the convolution integral (see *Carslaw and Jaeger* [1990, chapter II, section 2.5] or *Jury and Roth* [1990, equation (2.51)])

$$T(z, t) = \int_0^t T(0, \tau) f_T(t - \tau, z) d\tau \quad (7)$$

with the kernel (transfer function)

$$f_T(t, z) = \frac{z}{2[\pi d_h t^3]^{1/2}} \exp\left(-\frac{z^2}{4d_h t}\right). \quad (8)$$

Under the premises of a medium with uniform thermal properties and of a purely conductive heat transport with negligible heat production, (8) allows us to project temperatures measured at the soil surface to any depth.

Obviously, the thermal dynamics of permafrost soils cannot be understood from conductive heat transport alone. Further dominating processes are the transitions of water between the solid, liquid, and vapor phase and the convective transport of heat either in the liquid or in the vapor phase. In (2) all the heat-producing processes are lumped into r_h . To quantify them from temperature measurements, we integrate (2) over the small element $[z_i, z_{i+1}] \times [t^j, t^{j+1}]$, which will eventually be determined by the spatial and temporal discretization of the data. Assuming c_h and d_h are constant, we obtain with (3) and (5)

$$\int_{t^j}^{t^{j+1}} \int_{z_i}^{z_{i+1}} r_h(z, t) dz dt = c_h \left[\int_{z_i}^{z_{i+1}} T(z, t^{j+1}) - T(z, t^j) dz - d_h \int_{t^j}^{t^{j+1}} T'(z_{i+1}, t) - T'(z_i, t) dt \right], \quad (9)$$

where T' denotes the derivative of T with respect to z . This integral may be evaluated approximately from measured temperature data using the trapezoidal rule for integration and central finite differences for the derivative. It represents the heat produced in the depth interval $[z_i, z_{i+1}]$ during the time interval $[t^j, t^{j+1}]$. We notice that c_h and d_h affect the estimated heat production rate in different ways in that c_h is a multiplication factor, while d_h determines the relative weights of temperature changes and heat fluxes. Uncertainties in the value of c_h thus only translate into an uncertain magnitude of $r_h(z, t)$, while uncertainties of d_h may change its entire form.

4. Analysis

In this section we first look at the soil freezing characteristic, which is of utmost importance for understanding the dynamics of freezing soils. Then, postulating uniform thermal properties for the soil, we estimate values for the constant parameters c_h and d_h . The value for c_h is obtained from (6), the one for d_h is obtained from fitting projections of measured surface temperatures to temperatures measured at the corresponding depths. We verify a posteriori that the assumption of uniform thermal properties is justified for this site. Finally, the estimated values are used together with the high-resolution temperature measurements to calculate the rate of heat production. Relating the heat production to corresponding changes in liquid water content and, in turn, comparing them with the high-resolution TDR data allows for an independent verification.

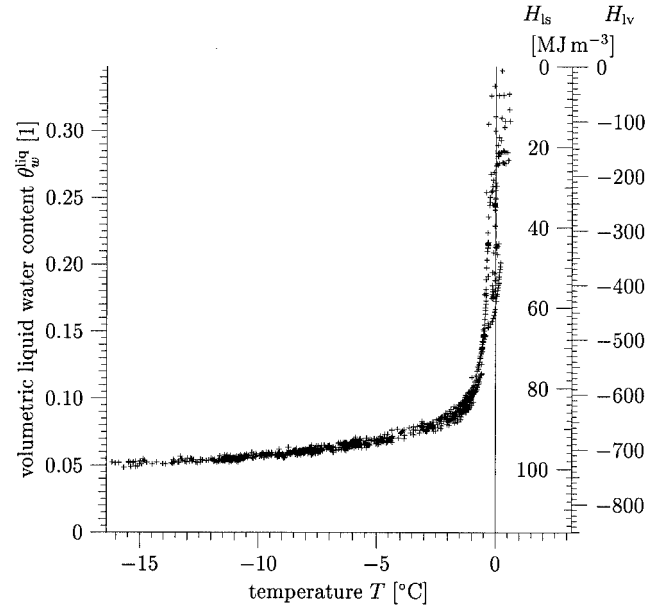


Figure 1. Empirical soil freezing characteristic obtained from plotting measured values of liquid water content versus temperature for the probes at 0.245 m depth. The axes on the right indicate the latent heat associated with the change of θ_w^{liq} if the excess water freezes (H_{ls}) or if it evaporates (H_{lv}). Notice that the origin of these axes is irrelevant, only differences matter.

4.1. Soil Freezing Characteristic

In a pure liquid, phase change occurs at a well-defined temperature. In contrast, a mixture of soil and water typically shows a rather smooth transition which is described by the soil freezing characteristic $\theta_w^{\text{liq}}(T)$ [*Yershov*, 1998]. Figure 1 shows the empirical soil freezing characteristic for the Bayelva site at a 0.245-m depth. For temperatures below -0.5°C , $\theta_w^{\text{liq}}(T)$ is a rather well-defined function, and, as a consequence, liquid water content may be expressed in terms of temperature. For T between -0.5 and 0°C , θ_w^{liq} does not only depend on T but also on the total water content. This may be understood as resulting from thermodynamic nonequilibrium which becomes stronger with increasing liquid water content because it takes more time to move the correspondingly larger amounts of latent heat. The data at other depths exhibit the same qualitative behavior with small vertical offsets.

It is worth noting that the measurements indicate a volume fraction of ~ 0.05 for liquid water at -15°C , which is comparable to the accuracy of the data. However, we recall the high clay content at this site and the fact that such high unfrozen water contents are generally encountered in fine-textured soils [*Farouki*, 1981] as well as in other porous materials [*Morishige and Kawano*, 1999]. In any case, for the present analysis a constant offset of the measurements, as it would most probably arise from using an inaccurate mixing model for inverting the TDR data, is immaterial since only differences of water contents are used.

4.2. Bulk Thermal Properties

On the basis of measured soil properties we estimate volume fractions $\{\theta_s, \theta_w, \theta_i\} = \{0.6, 0.05, 0.3\}$ for a frozen soil. Together with densities $\{\rho_s, \rho_w, \rho_i\} = \{2.65, 1.0, 0.91\} \times 10^3 \text{ kg m}^{-3}$ and specific heat capacities $\{c_{hs}, c_{hw}, c_{hi}\} =$

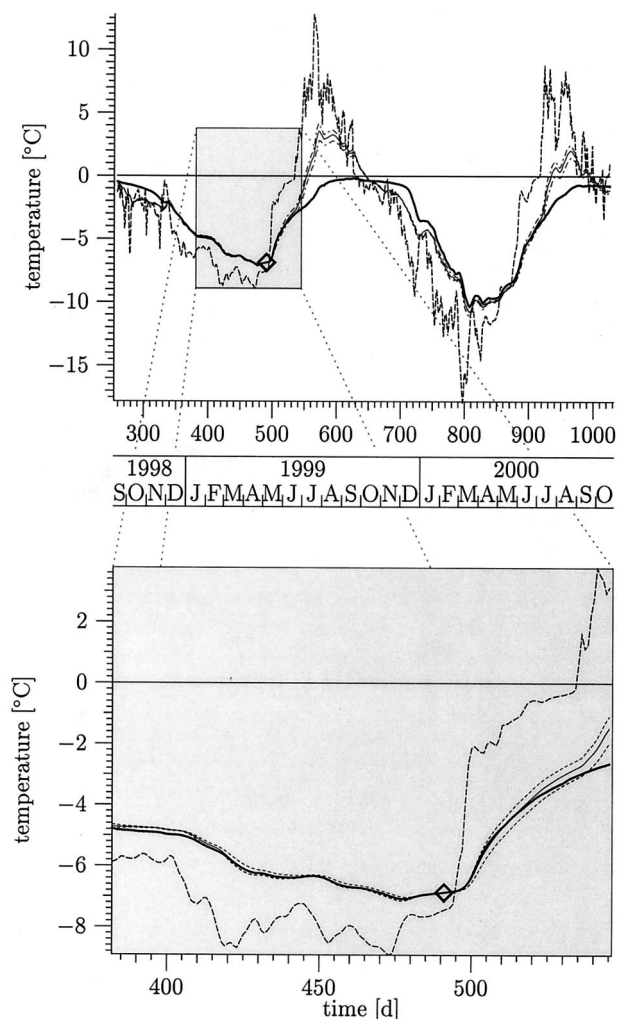


Figure 2. Measured temperatures at depths of 0.065 m (dashed line) and 1.25 m (thick solid line) together with projections of 0.065 m temperature to 1.25 m depth (thin solid line) using (7) and (8) with $d_h = 8 \times 10^{-7} \text{ m}^2 \text{ s}^{-1}$. The dashed-dotted lines are projections with d_h changed by $\pm 20\%$. Projected temperatures are matched to a measurement at the time indicated by the diamond. The top graph shows the entire data set; the bottom graph is the enlarged section outlined in the top graph.

$\{0.733, 4.22, 2.11\} \times 10^3 \text{ J kg}^{-1} \text{ K}^{-1}$ we obtain with (6) the estimate $c_h^{\text{frozen}} = 2.0 \times 10^6 \text{ J m}^{-3} \text{ K}^{-1}$ for the bulk volumetric heat capacity of the frozen soil. For the thawed soil with $\{\theta_s, \theta_w, \theta_i\} = \{0.6, 0.3, 0.0\}$ we similarly obtain $c_h^{\text{thawed}} = 2.4 \times 10^6 \text{ J m}^{-3} \text{ K}^{-1}$. In these calculations, we neglected the contribution of soil air because of its very low mass density. Hereinafter we will use the average value $c_h = (2.2 \pm 0.2) \times 10^6 \text{ J m}^{-3} \text{ K}^{-1}$.

As shown by (7) and (8), for pure heat conduction the temperature at depth z depends only on the temperature history of the soil surface and on the thermal diffusivity d_h . To estimate d_h , we choose a time interval during which nonconductive processes are presumably negligible. The surface soil temperature is approximated by the values measured by the topmost probe at a depth of 0.065 m. (Notice that because of snow cover and boundary effects this is a much better choice

than the air temperature recorded at a 2-m height at the weather station.) The value of d_h is then adjusted such that the temperature projected to a depth of 1.25 m, the location of the deepest probe, is in optimal agreement with the actual measurements (Figure 2). To do this, we can adjust two parameters: the thermal diffusivity d_h and a constant temperature shift. The constant shift accounts for the initial condition that is different from $T = 0^\circ\text{C}$ and for nonconductive processes in the time between $t = 0$, the start of the measurements, and the time when the profile was completely frozen. We chose a time with a sufficiently low temperature as a matching point (diamond in Figure 4). As is apparent from the graph, the value of the essential free parameter d_h is not sensitive to the choice of this point as long as the temperature is sufficiently low. It could have been chosen anywhere between $t = 400$ days and $t = 500$ days. Setting $d_h = 8 \times 10^{-7} \text{ m}^2 \text{ s}^{-1}$ gives an excellent agreement for the time interval where temperatures are significantly below 0°C and most of the soil water is frozen. This compares favorably with values calculated by Yershov [1998, p. 284] which for frozen silty clay loess are in the range $5.5 \times 10^{-7} - 8 \times 10^{-7} \text{ m}^2 \text{ s}^{-1}$.

Obviously, this method cannot be used to project temperatures across a thawing or freezing front. Consequently, values calculated for the thawed period deviate considerably from the measurements. It is interesting, however, that the same projection without any further adjustments is able to describe reasonably well the temperatures for the following frozen period, as is shown in the top graph of Figure 4.

Estimating d_h for the nonfrozen soil is impaired (1) by the short time intervals and shallow depths where the soil is actually thawed and (2) by the heat consumed by evaporation from the soil surface. However, at least for short periods, the value $d_h = 8 \times 10^{-7} \text{ m}^2 \text{ s}^{-1}$ again leads to excellent agreement between projected and measured temperatures. This is illustrated in Plate 3, which displays the difference between measured and projected temperatures for the entire soil profile during periods where heat conduction is the dominating process. Apparently, effective heat conduction at this site may be described by a constant thermal diffusivity, at least for periods and regions without strong phase transitions. This gives a posteriori justification to our initial assumption of a uniform medium. Although we cannot say anything about bulk thermal parameters when the transitions between phases dominate the thermal regime, we presume that the value of d_h is not affected significantly. Thus we will hereinafter use $d_h = 8 \times 10^{-7} \text{ m}^2 \text{ s}^{-1}$ and roughly estimate its uncertainty from Figure 4 as 20%.

Figure 3 shows the kernel (8) for $d_h = 8 \times 10^{-7} \text{ m}^2 \text{ s}^{-1}$. It illustrates that fluctuations of the surface temperature can travel rapidly through the soil: The maximum value of f_T at 0.6 m depth is reached after < 1 day, and at 1.2 m it is reached after merely 3.5 days. On the other hand, the time over which the surface forcing is integrated increases rapidly with depth, as is apparent from the very long tail.

4.3. Conductive Heat Flux

The mean value theorem applied to (3) for the conductive heat flux through some depth $z_{i+1/2}$ with $z_i < z_{i+1/2} < z_{i+1}$ yields

$$j_h(t, z_{i+1/2}) = -k_h \frac{T(t, z_{i+1}) - T(t, z_i)}{z_{i+1} - z_i}. \quad (10)$$

Choosing $z_{i+1/2} = [z_i + z_{i+1}]/2$, this becomes the traditional finite difference approximation (Plate 4). The value of

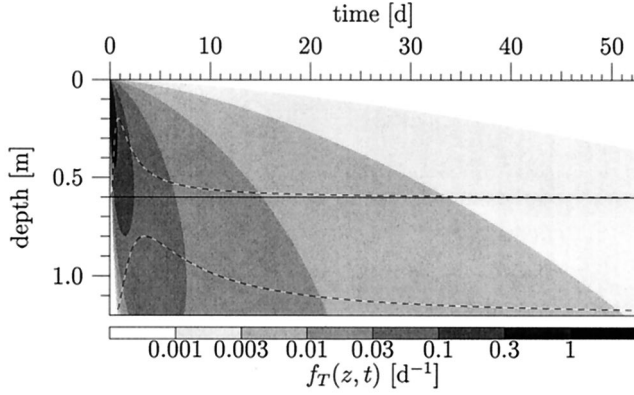


Figure 3. Transfer function $f_T(z, t)$, the normalized response of soil temperature to a narrow impulse perturbation at the surface, defined in (8) for $d_h = 8 \times 10^{-7} \text{ m}^2 \text{ s}^{-1}$. The two dashed lines represent cuts of $f_T(z, t)$ for depths of 0.6 and 1.2 m.

$k_h = c_h d_h$ is obtained from the estimates of c_h and d_h as $1.7 \text{ W m}^{-1} \text{ K}^{-1}$ with a relative error of 30%. This again compares favorably with the results of *Yershov* [1998], who gives values of $1.2\text{--}1.6 \text{ W m}^{-1} \text{ K}^{-1}$ for a frozen silty clay loess. Compared with the uncertainty of k_h , the errors of the temperature measurements and their locations are negligible. We notice that the uncertainty of k_h affects the magnitude of the estimate of j_h but not its form. In contrast, the choice $z_{i+1/2} = [z_i + z_{i+1}]/2$ does not affect the magnitude, but it leads to a local distortion of the form in that the position where (10) applies in reality shifts between z_i and z_{i+1} depending on the magnitude and direction of j_h .

4.4. Production of Latent Heat

We define the mean production of latent heat in the element $[z_i, z_{i+1}] \times [t^j, t^{j+1}]$, where z_i and z_{i+1} are the depths of adjacent temperature probes and t^j and t^{j+1} are successive measurement times, by

$$\bar{r}_{h_i}^j = \frac{1}{[t^{j+1} - t^j][z_{i+1} - z_i]} \int_{t^j}^{t^{j+1}} \int_{z_i}^{z_{i+1}} r_h(z, t) dz dt. \quad (11)$$

The integral is estimated using (9) with the spatial derivative T' approximated by finite differences. The value of $\bar{r}_{h_i}^j$ is assigned to the center of the element. Estimating \bar{r}_h for the depth interval $[z_i, z_{i+1}]$ thus requires temperature measurements at the four depths of z_{i-1} , z_i , z_{i+1} , and z_{i+2} . Plate 5 shows \bar{r}_h for two choices of the parameters c_h and d_h , namely for the upper and lower limits of their respective uncertainty band. To facilitate the later discussion, \bar{r}_h is also expressed as the equivalent rate \bar{r}_w of water undergoing phase change, which we define as

$$\bar{r}_w^{\alpha\beta} := \frac{\bar{r}_h}{L_{\alpha\beta}}, \quad (12)$$

where $L_{\alpha\beta}$ is the enthalpy of the transition from phase α to phase β . Values used are $L_{sl} = 0.333 \text{ MJ kg}^{-1}$, $L_{lv} = 2.45 \text{ MJ kg}^{-1}$, and $L_{sv} = 2.78 \text{ MJ kg}^{-1}$, where s , l , and v stands for solid, liquid, and vapor, respectively.

4.5. Importance of Latent Heat and Conduction

We consider stationary solutions of (2) in a uniform soil layer with constant r_h for the case where the boundaries are

maintained at the same constant temperature. With the layer extending between $-\ell/2$ and $+\ell/2$, where ℓ is a characteristic length, we obtain $j_h(z) = r_h z$, where we have set the integration constant to 0. For a stationary situation the heat flux thus varies proportionally to r_h in each uniform layer. On this basis we define the dimensionless number $R := r_h \ell / j_h$. We recognize that R is the ratio between the change of heat flux over the distance ℓ resulting from r_h and the total conductive heat flux. Hence we use R as a measure for the relative contributions of latent heat and conductive flux to the thermal dynamics. Plate 6 shows the estimate

$$R_i^j := \frac{\bar{r}_{h_i}^j \ell}{\bar{j}_{h_i}^j}, \quad (13)$$

where \bar{r}_h is defined in (11); ℓ is taken from Figure 8 as 0.4 m, the typical width of the layer where latent heat is consumed in the cold period; and $\bar{j}_{h_i}^j$ is the average heat flux over the time interval $[t^j, t^{j+1}]$.

5. Discussion

The thermal and the hydraulic dynamics of a permafrost soil's active layer are strongly coupled and run through characteristically different stages during the annual freeze-thaw cycle. The aim of the following discussion is (1) to decipher and to quantify the contributing processes from temperature measurements and (2) to corroborate the findings with measurements of the liquid water content.

At this site we may distinguish four periods in the phenomenology of the thermal dynamics: (1) the ‘‘cold period’’ between the cold front and the transition to positive (incoming) heat fluxes, which approximately coincides with the onset of snow melt, (2) the ‘‘warming period’’ between the transition to positive heat fluxes and the thawing front, (3) the ‘‘thawed period’’ between the thawing front and the zero curtain, and (4) the ‘‘isothermal plateau’’ between the zero curtain and the cold front. Each has its characteristic dynamics which has already been described by others in a qualitative manner [e.g., *Hinkel and Outcalt*, 1994, 1995; *Putkonen*, 1998]. In sections 5.1–5.5 we consider these periods individually and quantify the relevant processes. As the basis we use Plate 2 for measured temperatures and liquid water contents, Plate 4 for the conductive heat flux and for the thermal gradient which is proportional to the flux, and Plate 5 for the production of heat.

5.1. Cold Period

The two cold periods covered by the data are roughly between days 340 and 500 and between days 700 and 880. During much of the first cold period the ground was covered by a thick layer of snow, which greatly reduced the heat exchange with the atmosphere. Thus cooling of the soil profile was rather moderate despite low air temperatures. Conductive heat fluxes in the measuring region during this period ranged between 0 and -6 W m^{-2} with a mean of -2.6 W m^{-2} . During most of the second cold period, snow cover was thin, and cooling of the soil profile was hence quite strong with heat fluxes exceeding -20 W m^{-2} at an average of -5.5 W m^{-2} .

As a consequence of the soil freezing characteristic, cooling of the profile requires the reduction of the liquid water content. The excess water may either freeze, or it may evaporate and migrate toward cooler regions where it condenses or freezes out. Freezing of liquid water releases latent heat and

hence counteracts cooling, whereas evaporation consumes latent heat and furthers cooling. The relative weight of the two processes depends on thermal diffusivity, the effective diffusion coefficient of water vapor, and the temperature gradient.

Looking at \bar{r}_h , we find strong consumption of heat at intermediate depths between 0.5 and 1 m and production above and below this zone. This is more pronounced in the second, colder period. Apparently, evaporation of excess water dominates at intermediate depths. The vapor diffuses toward the cooler layers above, supposedly also into the snow cover, where the latent heat is deposited. Inspection of the data shows that between days 340 and 480, θ_w^{liq} decreased by ~ 0.03 , corresponding to 30 kg m^{-3} . To evaporate this mass, some 73 MJ of heat are required per cubic meter of soil. For the 140 days this leads to an average power density of some -6 W m^{-3} . For the second period, θ_w^{liq} decreased by ~ 0.04 between days 720 and 810, which leads to an average power density during this time interval of about -13 W m^{-3} . These numbers agree reasonably well with the calculations shown in Plate 5. The analysis was corroborated qualitatively by observations during a spring field trip which revealed a thick layer of depth hoar, large, beautiful snow crystals, at the bottom of the snow. This is interpreted as an indication of vapor migration into the snow. Direct measurements of vapor flux out of the ground have been reported for other sites [e.g., Santeford, 1978; Woo, 1982].

While we can at least estimate an upper limit for the amount of water evaporating from depths between 0.5 and 1 m from the TDR measurements and thereby corroborate the calculation of \bar{r}_h , this is not possible for the amount of condensing and freezing water vapor since it does not manifest itself in a change of the liquid water content. Still, we may estimate a lower bound for the amount of water transferred to the depth interval of 0.32–0.45 m between days 700 and 800 from \bar{r}_h . Inspection of the data yields $\bar{r}_h = 4.7 \pm 1.6 \text{ W m}^{-3}$ for this interval, where the uncertainty stems from the parameters c_h and d_h . This corresponds to the freezing of $15 \pm 5 \text{ kg}$ of water per cubic meter of soil during these 100 days.

The nature of the heat production at depths below 1 m during the cold period is less obvious. We interpret this as resulting from freezing or condensing water in the absence of appreciable vapor migration and hence of negligible evaporation. We suggest one reason for this is that during the thawed period, liquid water content at this site is maximal at depths between 0.8 and 1 m. Compared with the shallower depths with lower water contents, this region may thus be expected to become less permeable for water vapor upon freezing. Support for this interpretation comes again from field observations. During the instrumentation of the site, a massive ice-rich layer without apparent pores was actually identified below $\sim 1 \text{ m}$. Accumulation of ice at the base of the active layer, i.e., at the top of permafrost, has been quantified and reported from field and laboratory experiments by others [e.g., Yershov, 1998; Solomatina and Xu, 1994].

As would be expected, the production of heat, which depends strongly on migration and condensation of water vapor, is modulated by fluctuations of the surface temperature. We noticed earlier that such fluctuations can penetrate the entire soil profile in a rather short time. Prolonged warmer periods, for instance, between days 430 and 440 or between days 805 and 815, reduce or even invert the thermal gradient and thus reduce the condensation rate. This is reflected in a strong decrease of the heat consumption in the source regions of water vapor at intermediate depth and in a corresponding

reduction of heat production in the drain regions above, as becomes particularly evident at later times of the cold period.

With temperatures still very low but rising after days 470 and 825, respectively, the processes discussed so far are reversed. From the surface, a temperature increase is forced, which releases frozen water according to the soil freezing characteristic and also increases the vapor content of the soil air. Melting and evaporation consumes heat, which counteracts the temperature increase. This heat is transported by the water vapor to deeper layers which are slightly cooler. Condensation and freezing, again in accordance with the soil freezing characteristic, releases this heat and warms the layers. As a consequence of this feedback, a uniform temperature profile develops, and the soil becomes warmer as a whole. The conductive heat flux, which is quite variable and changes its sign several times with depth, corroborates our interpretation. Apparently, this process reaches only down to $\sim 1 \text{ m}$ as is indicated by \bar{r}_h and by inspection of the temperature data, which show the warming of the profile below 1 m to lag behind that of the layers above. The less permeable soil layer suggested above would also explain this result.

We notice that our findings of the dynamics of the frozen active layer contrasts those of other sites for which it was stipulated that upon closing of the zero curtain, internal distillation and water advection cease for the rest of the winter [Hinkel and Outcalt, 1994; Romanovsky and Osterkamp, 2000].

5.2. Warming Period

With average daily air temperatures above 0°C after days 498 and 872, respectively, the conductive heat flux turned positive throughout the observed soil profile. It remained rather weak during the warming period, however, with a mean of 4.4 W m^{-2} at an average net radiation of 16.5 W m^{-2} for the interval between days 500 and 530. The corresponding numbers for the interval between days 880 and 915 are 5.7 W m^{-2} for the average conductive heat flux and 26.6 W m^{-2} for the average net radiation. The large difference between these fluxes reflects the heat consumed by the melting of the snow cover.

The onset of the first warming period is characterized by a rapid increase of the air temperature from -14°C to $+1^\circ\text{C}$ within 48 hours. The topmost temperature probe responded with an increase from -7°C to -3°C within 5 days. According to the soil freezing characteristic, this warming increases θ_w^{liq} by ~ 0.015 , which is confirmed by the TDR measurements, and consumes $\sim 5 \text{ MJ m}^{-3}$ soil corresponding to $\bar{r}_h \approx -11 \text{ W m}^{-3}$. However, instead of a consumption we find a release with \bar{r}_h of the order of $+20 \text{ W m}^{-3}$ down to a depth of 0.9 m. This is explained by the dynamics of the snow cover. Temperature measurements, which are not reported here, show that it warmed between days 491 and 495 and was isothermal between days 495 and 500. This may even have generated some meltwater that could rapidly infiltrate the soil through cracks. In any case, the greatly increased temperature enforced a downward vapor flux toward the colder layers. While we cannot estimate the relative weight of these two processes, we can calculate the mass of water required for each of them to reproduce the observation that \bar{r}_h is some 30 W m^{-3} larger than expected without movement of water. For the 5-day period between days 498 and 503 the freezing of some 38 kg of water per cubic meter of soil would be required if infiltrating meltwater was the only cause. Conversely, if we assume only vapor movement, some 4.5 kg m^{-3} would suffice. This corresponds to

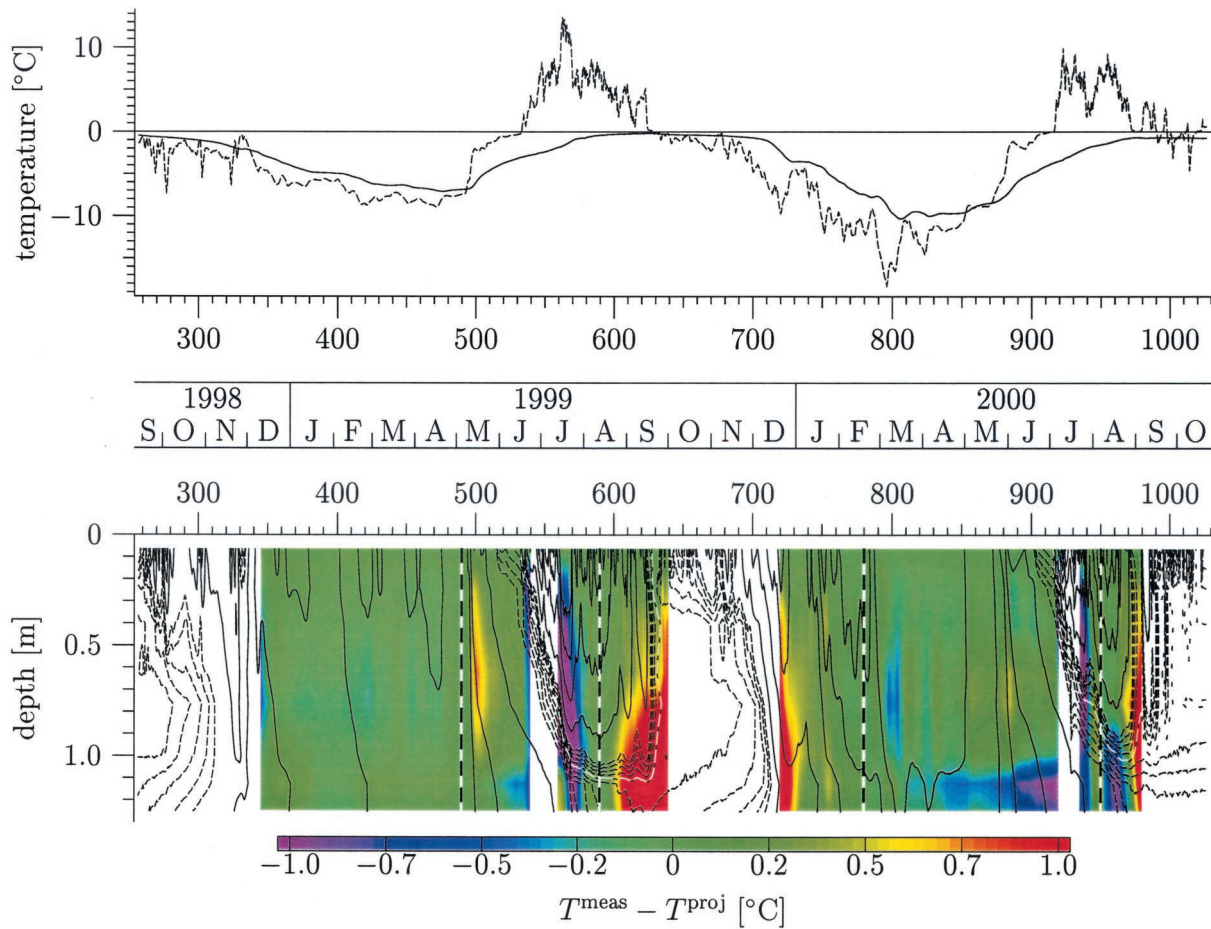


Plate 3. Difference between measured and projected temperatures for periods with dominating heat conduction. Projection is from a depth of 0.065 m using (7) and (8) with $d_h = 8 \times 10^{-7} \text{ m}^2 \text{ s}^{-1}$. Along the vertical patterned lines, measured and projected temperatures were matched. Open areas indicate time intervals where projection is not permissible because of a strong influence of phase transitions. Measured temperatures in the shallowest probe at 0.065 m (dashed line) and of the deepest probe at 1.25 m (solid line) are shown in the top frame.

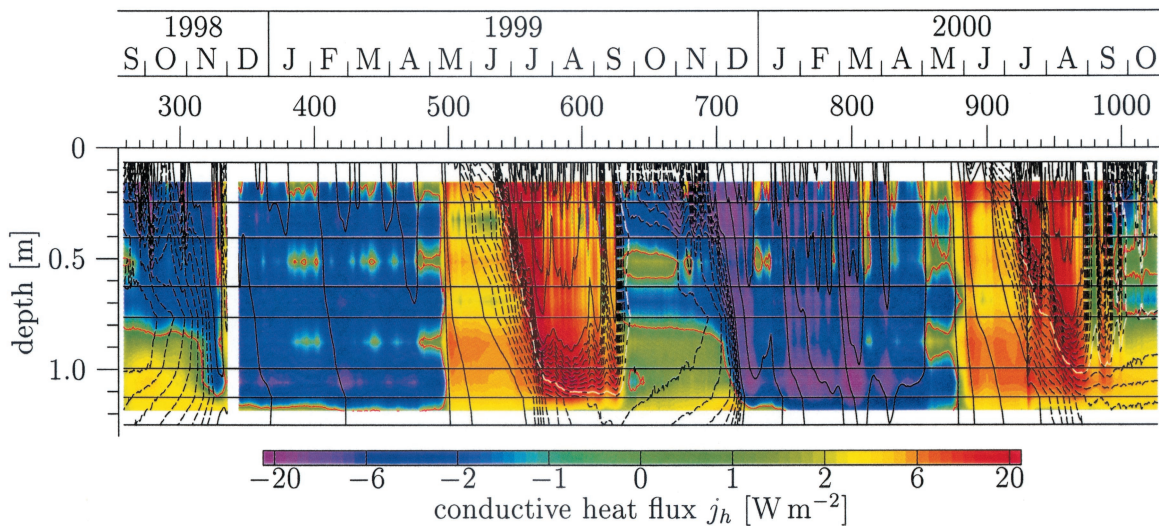


Plate 4. Conductive heat flux estimated from the centered finite difference approximation of (3). Black contour lines are for temperature and the red contour is $j_h = 0$. Horizontal lines indicate the depths for which j_h was estimated, and open areas correspond to missing data. Notice the logarithmic scale.

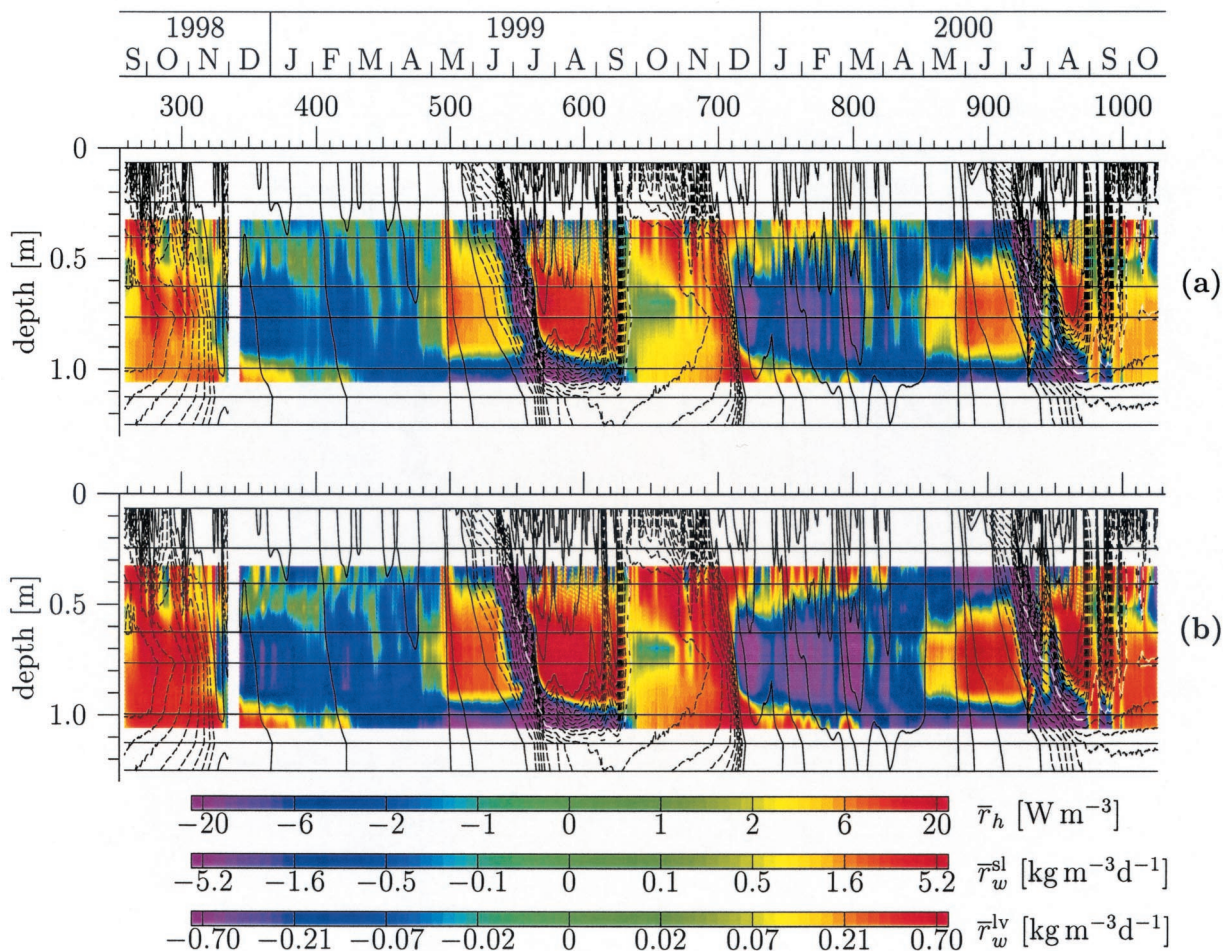


Plate 5. Production of latent heat estimated from (9) for (a) lower and (b) upper bounds of c_h and d_h . Horizontal black lines indicate the depth of temperature probes. As an aid for interpretation, color bars are given for $\bar{\tau}_h$, as well as for equivalent rates of water in a solid to liquid ($\bar{\tau}_w^{sl}$) and a liquid to vapor ($\bar{\tau}_w^{lv}$) phase change.

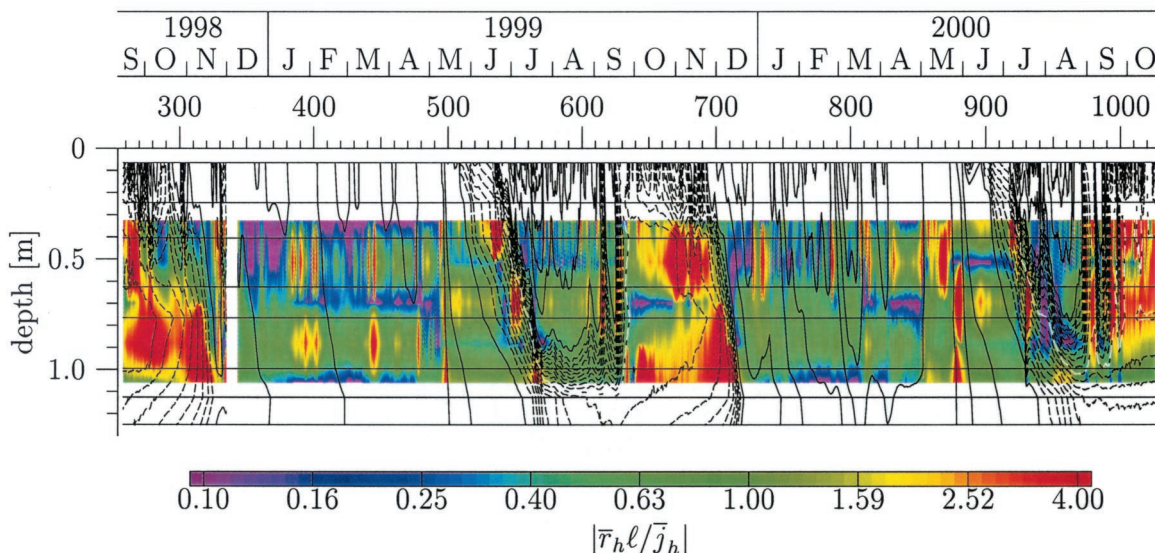


Plate 6. Dimensionless ratio between contributions to thermal dynamics originating from production of latent heat and from heat conduction.

an increase of the volumetric ice content by ~ 0.042 and 0.005 , respectively. Both extremes could easily be generated by the melting snow cover. We comment that infiltrating snowmelt water has been observed in many field studies and that the corresponding warming of soil down to greater depths has been attributed to refreezing meltwater [e.g., *Thunholm et al.*, 1989; *Woo and Marsh*, 1990; *Marsh and Woo*, 1993]. *Hinkel and Outcalt* [1994] also postulate that rapid warming of soil is caused by meltwater and downward migration of vapor.

By day 505, average daily air temperature returned to $\sim 0^\circ\text{C}$ for some 25 days, presumably stabilized by the thawing of the snow cover. The concurrent warming of the soil thus reduced the thermal gradient and with it the vapor flux. The advancing thawing front finally pushed the source region for the water vapor deeper into the soil with the drain region bounded by the less permeable layer at 0.9 m depth.

Below 0.9 m the heat consumed by the melting of water required by the soil freezing characteristic is not compensated by condensing vapor. Inspection of the data shows that during the period between days 500 and 550, θ_w^{liq} increases by 0.025, which leads to the estimate $\bar{r}_h \approx 2 \text{ W m}^{-3}$. The average value calculated for this time interval and for $z > 1 \text{ m}$ is $2.5 \pm 1.1 \text{ W m}^{-3}$, which is in excellent agreement with the measurements.

The dynamics during the second warming period is qualitatively identical to the first one and is not discussed any further here.

5.3. Thawed Period

The thawing front which starts this period is a macroscopic phase boundary between the partly frozen and the completely thawed soil. We distinguish it from the microscopic phase boundaries, which exist in the partly frozen zone, because the latent heat associated with the transition $T \rightleftharpoons T - \Delta T$ is much larger for $T = 0^\circ\text{C}$ than for subzero temperatures (Figure 1). As a consequence, the macroscopic phase boundary stabilizes the temperature against much larger heat fluxes, and thereby behaves more like a classical sharp phase boundary, than is the case for its microscopic counterpart.

As expected, we find the highest heat consumption rates in the rather narrow thawing front. Inspection of the data yields for the first thawing front, which we define as the region with $-0.6 < T [^\circ\text{C}] < 0$ between days 530 and 570, an average power density of $-40 \pm 13 \text{ W m}^{-3}$. The corresponding value for the second thawing front between days 910 and 960 is $-32 \pm 10 \text{ W m}^{-3}$. The consumption of heat in the thawing front reflects the net effect of three processes: (1) the thawing of the remaining frozen water, (2) the evaporation of water vapor which migrates to layers below the thawing front, and (3) the condensation of water vapor migrating downward from the warmer, already thawed soil above. The first two processes consume heat, whereas the third one produces heat. From the data available here it is not possible to reliably calculate the amounts of water involved in each of the processes.

We now consider the situation at depths greater than $\sim 1 \text{ m}$. As already suggested in section 5.1, the migration of water vapor at these depths is severely impeded. On the basis of this premise we calculate the change of θ_w^{liq} from \bar{r}_h . Inspection of the data yields for the period between days 570 and 620 an average power density of $-7.7 \pm 2.5 \text{ W m}^{-3}$. Using (12), we calculate from this an increase of 0.10 ± 0.03 for θ_w^{liq} during this time. The TDR measurements actually show an increase of 0.10.

Turning to the actually thawed region, we find a strong production of heat for depths below $\sim 0.4 \text{ m}$. The only process to generate it is the condensation of water vapor that originated at shallower, warmer depths and migrated toward the colder layers. The data give $18 \pm 5.5 \text{ kg m}^{-2}$ for the amount of water that is transferred in this process. The measurements of θ_w^{liq} support this interpretation if we make the reasonable assumption that after condensation the water flowed to the base of the thawed zone, where it accumulated. This downward migration of moisture is also supported by the TDR data.

We notice that during the thawed period a large portion of the net radiation, 25–70%, is consumed for evaporating water from the soil surface [*Ohmura*, 1982; *Rouse et al.*, 1977; *Boike et al.*, 1998]. This loss of water from the surface layer is compensated by rainfall and by the capillary rise of liquid water from greater depths. Inspection of the TDR data reveals that at our site the source region for the capillary rise reaches to a depth of only $\sim 0.3 \text{ m}$. In a shallow zone we thus find water fluxes to be strongly transient, upward and downward, driven by atmospheric forcing. At greater depths, water flux is always downward: vapor migration toward lower temperatures and liquid migration in the gravity field.

The two thawed periods covered by the data are qualitatively similar. Quantitative differences resulted from the weather patterns, for instance, when a cold episode in the second period interrupted and delayed the thawing front for a few days. We notice that, again, as during the cold period, fluctuations of the air temperature rapidly propagate through the completely thawed zone and are stopped only by the thawing front which constitutes a macroscopic phase boundary. Temperatures in the thawed zone thus follow the air temperatures as described by (7).

With air temperatures decreasing, the thawed zone cools and eventually reaches 0°C . Freezing sets in and the dynamics becomes controlled by other processes.

5.4. Isothermal Plateau

The closing of the zero curtain may be interpreted as the rapid movement of the macroscopic phase boundary from the bottom of the completely thawed region to the soil surface. Compared with the reverse movement, i.e., the penetration of the thawing front, this is a fast phenomenon because only a small fraction of the water is involved in the associated phase change. With further cooling of the soil surface the macroscopic phase boundary advances into the soil as a cold front.

The macroscopic phase boundary prevents temperature fluctuations from the surface to reach greater depths. As a consequence, temperatures stay near 0°C , and conductive heat fluxes are very small. For instance, the average of j_h in the region where $-0.2 < T [^\circ\text{C}] < 0$ is only -0.6 W m^{-2} . While conductive processes are thus practically negligible, the production of heat from the freezing of water is not. For the interval between the depths of 0.31 and 1.03 m and the temperatures $-0.2^\circ < T < 0^\circ$ ($^\circ\text{C}$), inspection of the data shows a decrease of the liquid water by 48 kg m^{-2} and for temperatures $-2^\circ < T < -0.2^\circ$ ($^\circ\text{C}$) a decrease by 124 kg m^{-2} . Calculating the same quantities from \bar{r}_h , we obtain 24 ± 7 and $126 \pm 38 \text{ kg m}^{-2}$, respectively. The significant difference for the first interval may be easily explained by water vapor that leaves the considered region. Indeed, after the discussion in section 5.3 we expect that part of the heat produced by freezing is immediately consumed by evaporating water. This vapor migrates toward colder zones where the heat is released again.

As Plate 5 shows, between days 630 and 670 a large part of the cold front is beyond the region where we can calculate \bar{r}_h , and we expect a significant loss of water vapor. Taking this into account, we find excellent agreement between measurements and calculations.

5.5. Why Does This Analysis Work?

The discussions in sections 5.1–5.4 emphasized the importance of latent heat production in all four periods. At first this appears to contradict the finding that temperatures at greater depths can be projected from measured surface temperatures assuming pure heat conduction (Plate 3). In order to resolve this we consider a homogeneous soil at $T < 0^\circ\text{C}$ and negligible movement of water.

We calculate the effective heat capacity from the energy δE required to change the temperature of a unit volume by an infinitesimal value δT . This is

$$\delta E(T) = \delta T \left[c_h + \frac{d\theta_w^{\text{liq}}(T)}{dT} \rho_w L_{sl} \right], \quad (14)$$

where the first term in brackets comes from the energy required for changing the temperature of the material, with c_h being the heat capacity defined in (6), and the second term comes from the energy consumed in the phase change. We neglect the small amount of energy associated with the corresponding change of the vapor content. The effective heat capacity thus becomes

$$c_h^{\text{eff}}(T) := \frac{\delta E(T)}{\delta T} = c_h + \frac{d\theta_w^{\text{liq}}(T)}{dT} \rho_w L_{sl}. \quad (15)$$

In the next step we calculate the production rate of latent heat associated with the rate of change of temperature. Using the chain rule of differentiation on the soil freezing characteristic, which we write as $\theta_w^{\text{liq}}(T(z, t))$, we obtain

$$r_h = \frac{d\theta_w^{\text{liq}}(T)}{dT} \frac{\partial T}{\partial t} \rho_w L_{sl}. \quad (16)$$

We now formulate the dynamics of the effective heat conduction in analogy to (2) as

$$\frac{\partial}{\partial t} [c_h^{\text{eff}}(T)T] + \frac{\partial}{\partial z} j_h = r_h, \quad (17)$$

we insert (15) and (16) and obtain, after some transformations using the product rule on $c_h^{\text{eff}}(T)T$ and, again, the chain rule,

$$\begin{aligned} & \frac{\partial}{\partial t} [c_h^{\text{eff}}(T)T] + \frac{\partial}{\partial z} j_h - r_h \\ &= c_h \frac{\partial}{\partial t} T \left[1 + T \frac{\rho_w L_{sl}}{c_h} \frac{d^2\theta_w^{\text{liq}}(T)}{dT^2} \right] + \frac{\partial}{\partial z} j_h = 0. \end{aligned} \quad (18)$$

The second term in the brackets results from the rate of change along the soil freezing characteristic with time. As can be seen from Figure 1, for sufficiently low temperatures the curvature of $\theta_w^{\text{liq}}(T)$ becomes very small. For our site the second term can actually be shown to be much smaller than 1 below about -2°C . Neglecting it, we recover

$$\frac{\partial}{\partial t} [c_h T] + \frac{\partial}{\partial z} j_h = 0, \quad (19)$$

which is the basis of (7) and (8). We thus find that for a homogeneous soil at sufficiently low temperatures and with negligible water fluxes, (19) gives an approximately correct description of the thermal dynamics even when production of latent heat is significant. This explains the success of the projections (7) and (8).

Finally, the apparent homogeneity with respect to effective thermal processes warrants some comments since, after all, this site is a classic example of patterned ground. We recall that the profile analyzed here is at the center of a mineral hummock and is thus much more uniform than one at the fringe where rather thick pockets of organic material are encountered. The very fine texture of the material adds to the homogeneity since total water content is roughly constant. Thermal capacity thus does not vary much over the year and through the profile, which may be seen from a short sensitivity analysis of (6). The case is not so simple with effective thermal diffusivity, as was mentioned in section 4.2. Avoiding speculations on its spatial and temporal variability, which are notoriously difficult to verify anyway, we base the assumption of a constant value of d_h on the success of projecting surface temperatures to deeper layers (Figure 2 and Plate 3). For cold periods the extent of agreement between measured and projected temperatures at all depths leaves little room for a possible variation of d_h . This is also true for the thawed periods, although to a lesser degree because the duration of the time series is much shorter. For periods with very strong phase changes the constant value of d_h is but a suggestion which we currently cannot check. This uncertainty obviously also extends to production rates of heat that are calculated using the constant value of d_h .

6. Summary and Conclusions

The thermal and hydraulic dynamics of a permafrost site was monitored over a period of 778 days in a depth interval between 0.06 and 1.25 m. We found it useful to separate the observed phenomenology into four sections: the cold period, the warming period, the thawed period, and the isothermal plateau.

We found that at this site, bulk thermal properties, in particular, heat capacity and thermal diffusivity, do not vary strongly, neither in time nor with depth. Also, the soil freezing characteristic was found to be invariant through the two freeze-thaw cycles observed so far.

We showed theoretically, in (14)–(19), that the effective thermal dynamics including phase transitions may be approximated by pure heat conduction, with the thermal properties assigned their bulk values, if (1) the mass movement of water is negligible and (2) temperatures are such that the curvature of the soil freezing characteristic is sufficiently small. The validity of this approximation was demonstrated by the successful prediction of the temperature in the entire soil profile from projections of measured near-surface temperatures. We concluded from this that the thermal properties at this site are approximately constant. Obviously, such a projection yields grossly wrong results when a macroscopic phase boundary lies between the measuring depth and the projection depth. We found, however, that reasonable prediction is possible even across time intervals during which such a boundary existed. In particular, temperatures fitted at some time during the first winter could be projected, using the forcing at the surface, to the next winter without any further adjustments.

Measurements of the soil temperature, together with the

constant bulk thermal parameters determined previously, enabled us to calculate conductive heat fluxes and heat production rates with high precision and high temporal resolution. From these calculations we could deduce and quantify the details of the thermal and hydraulic dynamics at this site. Independent quantitative verification was possible through measured liquid water contents. We remark that a crucial prerequisite for our analysis is a profile of calibrated temperature sensors with a high accuracy since unbiased estimates of spatial derivatives up to order 2 are required. Once such a measurement chain is established, it provides a very sensitive instrument for reliably detecting heat fluxes and releases of latent heat in the active layer of a permafrost soil.

We found that the production of latent heat and the associated migration of water vapor is an important agent in the thermal dynamics at this site for all four periods and that it is the dominating process in the isothermal plateau since heat conduction is practically negligible there. We further deduced from the measurements that practically unimpeded vapor migration is possible down to some 0.9 m. Below that depth, vapor migration was found to be severely restricted by a massive ice-rich layer. Although the amounts of water involved in the migration of latent heat were generally rather small, the large value of the enthalpy of evaporation, which is larger than that of melting by a factor of 7.4, makes vapor an efficient means for the transport of thermal energy.

Acknowledgments. We gratefully acknowledge financial support by the Deutsche Forschungsgemeinschaft (Ro 1080/4-1&2), the European Union (LSF grant NP-98-5), and a research grant awarded to Julia Boike (BMBF-LPD 9901/8-11) by the Deutsche Akademie der Naturforscher Leopoldina. Essential logistic support was provided by the German and the Norwegian Research Stations in Ny-Ålesund. Pier Paul Overduin and Olaf Ippisch were indispensable for the initial instrumentation of the site and for creating and maintaining the database. We gratefully acknowledge the constructive and very helpful comments of two anonymous reviewers.

References

- Boike, J., K. Roth, and P. P. Overduin, Thermal and hydrologic dynamics of the active layer at a continuous permafrost site (Taymyr Peninsula, Siberia), *Water Resour. Res.*, **34**, 355–363, 1998.
- Carslaw, H. S., and J. C. Jaeger, *Conduction of Heat in Solids*, 2nd ed., Oxford Univ. Press, New York, 1990.
- Chen, G., and E. J. Chamberlain, Observations of moisture migration in frozen soils during thawing, in *Fifth International Conference on Permafrost*, vol. 1, edited by K. Senneset, pp. 308–312, Tapir, Trondheim, Norway, 1988.
- Costard, F., Mars: The periglacial planet, *Astronomie*, **102**, 80–90, 1988.
- Crank, J., *The Mathematics of Diffusion*, 2nd ed., Oxford Univ. Press, New York, 1975.
- Farouki, O. T., Thermal properties of soils, *Monogr. 81-1*, U.S. Army Cold Reg. Res. and Eng. Lab., Hanover, New Hampshire, 1981.
- Førland, E. J., I. Hanssen-Bauer, and P. O. Nordli, Climate statistics and longterm series of temperature and precipitation at Svalbard and Jan Mayen, *Rep. 21/97 KLIMA*, Norwegian Meteorol. Inst., Oslo, 1997.
- French, H. M., *The Periglacial Environment*, 2nd ed., Addison-Wesley-Longman, Reading, Mass., 1996.
- Hallet, B., Self-organization in freezing soils: From microscopic ice lenses to patterned ground, *Can. J. Phys.*, **68**, 842–852, 1990.
- Hassanizadeh, S. M., and W. G. Gray, General conservation equations for multi-phase systems, **2**, Mass, momenta, energy and entropy equations, *Adv. Water Res.*, **2**, 191–203, 1979.
- Hinkel, K. M., and S. I. Outcalt, Detection of nonconductive heat transport in soils using spectral analysis, *Water Resour. Res.*, **29**, 1017–1023, 1993.
- Hinkel, K. M., and S. I. Outcalt, Identification of heat-transfer processes during soil cooling, freezing, and thaw in Central Alaska, *Permafrost Periglacial Processes*, **5**, 217–235, 1994.
- Hinkel, K. M., and S. I. Outcalt, Detection of heat-mass transfer regime transitions in the active layer using fractal geometric parameters, *Cold Reg. Sci. Technol.*, **23**, 293–304, 1995.
- Hinkel, K. M., S. I. Outcalt, and F. E. Nelson, Near-surface summer heat-transfer regimes at adjacent permafrost and non-permafrost sites in Central Alaska, in *Proceedings of the Sixth International Conference on Permafrost*, pp. 261–266, South China Univ. of Technol. Press, Beijing, 1993.
- Huang, S., H. N. Pollack, and P.-Y. Shen, Temperature trends over the past five centuries reconstructed from borehole temperatures, *Nature*, **403**, 756–758, 2000.
- Jury, W. A., and K. Roth, *Transfer Functions and Solute Movement Through Soils: Theory and Applications*, Birkhäuser Boston, Cambridge, Mass., 1990.
- Kane, D. L., R. E. Gieck, and L. D. Hinzman, Evapotranspiration from a small Alaskan arctic watershed, *Nordic Hydrol.*, **21**, 253–272, 1990.
- Krantz, W. B., Self-organization manifest as patterned ground in recurrently frozen soils, *Earth Sci. Rev.*, **29**, 117–130, 1990.
- Liestøl, O., Pings, springs and permafrost in Spitsbergen, Årbok 1975, Norsk Polarinstitut, Tromsø, Norway, 1977.
- Marsh, P., and M.-K. Woo, Infiltration of meltwater into frozen soils in a continuous permafrost environment, in *Proceedings of the Sixth International Conference on Permafrost*, pp. 443–448, South China Univ. of Technol. Press, Beijing, 1993.
- Morishige, K., and K. Kawano, Freezing and melting of water in a single cylindrical pore: The pore-size dependence of freezing and melting behavior, *J. Chem. Phys.*, **110**, 4867–4872, 1999.
- Ohmura, A., Climate and energy balance on the arctic tundra, *J. Climate*, **2**, 65–84, 1982.
- Outcalt, S. I., F. E. Nelson, and K. M. Hinkel, The zero-curtain effect: Heat and mass transfer across an isothermal region in freezing soil, *Water Resour. Res.*, **26**, 1509–1516, 1990.
- Outcalt, S. I., K. M. Hinkel, F. E. Nelson, and L. L. Miller, Estimating the magnitude of coupled-flow effects in the active layer and upper permafrost, Barrow, Alaska U.S.A., in *Proceedings of Seventh International Conference on Permafrost*, pp. 869–873, Centre d'Études Nordiques, Quebec, Canada, 1998.
- Overpeck, J., et al., Arctic environmental change of the last four centuries, *Science*, **278**, 1251–1256, 1997.
- Parmuzina, O. Y., Cryogenic texture and some characteristics of ice formation in the active layer (in Russian), in *Problems of Cryolithology*, edited by A. I. Popov, vol. 7, pp. 131–152, Moscow Univ. Press, Moscow, 1978. (English translation *Polar Geogr. Geol.*, 131–152, 1980.)
- Philip, J. R., and D. A. de Vries, Moisture movement in porous materials under temperature gradients, *Eos Trans. AGU*, **38**, 222–232, 1957.
- Putkonen, J., Soil thermal properties and heat transfer processes near Ny-Ålesund, northwestern Spitsbergen, Svalbard, *Polar Res.*, **17**, 165–179, 1998.
- Ray, R. J., W. B. Krantz, T. N. Caine, and R. D. Gunn, A model for sorted patterned-ground regularity, *J. Glaciol.*, **29**, 317–337, 1983.
- Romanovsky, V. E., and T. E. Osterkamp, Effects of unfrozen water on heat and mass transport processes in the active layer and permafrost, *Permafrost Periglacial Processes*, **11**, 219–239, 2000.
- Roth, K., R. Schulin, H. Flüßler, and W. Attinger, Calibration of time domain reflectometry for water content measurement using a composite dielectric approach, *Water Resour. Res.*, **26**, 2267–2273, 1990.
- Rouse, W. R., Microclimate of arctic tree line, **2**, Soil microclimate of tundra and forest, *Water Resour. Res.*, **20**, 67–73, 1984.
- Rouse, W. R., P. F. Mills, and R. B. Stewart, Evaporation in high latitudes, *Water Resour. Res.*, **13**, 909–914, 1977.
- Santeford, H. S., Snow soil interaction in interior Alaska, in *Modeling of Snow Cover Runoff*, edited by S. C. Colbeck and M. Ray, pp. 311–318, Cold Reg. Res. and Eng. Lab., Hanover, New Hampshire, 1978.
- Serreze, M. C., J. E. Walsh, F. S. Chapin, T. Osterkamp, M. Dyurgerov, V. Romanovsky, W. C. Oechel, J. Morison, T. Zhang, and R. G. Barry, Observational evidence of recent change in the northern high-latitude environment, *Clim. Change*, **46**, 159–207, 2000.
- Solomatina, V. I., and X. Xu, Water migration and ice segregation in

- the transition zone between thawed and frozen soil, *Permafrost Periglacial Processes*, 5, 185–190, 1994.
- Thunholm, B., L.-C. Lundin, and S. Lindell, Infiltration into a frozen heavy clay soil, *Nordic Hydrol.*, 20, 153–166, 1989.
- Woo, M.-K., Upward flux of vapor from frozen materials in the high Arctic, *Cold Reg. Sci. Technol.*, 5, 269–274, 1982.
- Woo, M.-K., and P. Marsh, Response of soil moisture change to hydrological processes in a continuous permafrost environment, *Nordic Hydrol.*, 21, 235–252, 1990.
- Yershov, E. D., *General Geocryology*, Cambridge Univ. Press, New York, 1998.
- Zuber, M. T., et al., Observations of the north polar region of Mars from the Mars orbiter laser altimeter, *Science*, 282, 2053–2060, 1998.
-
- J. Boike, Water and Environmental Research Center, University of Alaska Fairbanks, P.O. Box 755860, Fairbanks, AK 99775. (ffjb2@uaf.edu)
- K. Roth, Institute of Environmental Physics, University of Heidelberg, D-69120 Heidelberg, Germany. (kurt.roth@iup.uni-heidelberg.de)

(Received December 22, 2000; accepted May 9, 2001.)